arXiv:nucl-ex/0011021v1 30 Nov 2000

# A linear radiofrequency ion trap for accumulation, bunching, and emittance improvement of radioactive ion beams

F. Herfurth [a,1], J. Dilling [a], A. Kellerbauer [b,e], G. Bollen [c], S. Henry [d], H.-J. Kluge [a], E. Lamour [a], D. Lunney [d], R. B. Moore [e], C. Scheidenberger [a], S. Schwarz [b,a], G. Sikler [a], J. Szerypo [f]

[a] *GSI, D-64291 Darmstadt, Germany*

[b] *CERN, CH-1211 Geneva 23, Switzerland*

[c] *Sekt. Phys., Ludwig-Maximilians-Univ. München, D-85748 Garching, Germany*

[d] *CSNSM-IN2P3-CNRS, F-91405 Orsay-Campus, France*

[e] *Dept. of Phys., McGill University, Montréal (Québec) H3A 2T8, Canada*

[f] *Dept. of Phys., Univ. of Jyväskylä, PB 35(Y5), FIN-40351 Jyväskylä, Finland*

PACS number: 21.10.Dr, 2.10.Bi, 07.75.+h

**Abstract**

An ion beam cooler and buncher has been developed for the manipulation of radioactive ion beams. The gas-filled linear radiofrequency ion trap system is installed at the Penning trap mass spectrometer ISOLTRAP at ISOLDE/CERN. Its purpose is to accumulate the 60-keV continuous ISOLDE ion beam with high efficiency and to convert it into low-energy low-emittance ion pulses. The efficiency was found to exceed 10 % in agreement with simulations. A more than 10-fold reduction of the ISOLDE beam emittance can be achieved. The system has been used successfully for first on-line experiments. Its principle, setup and performance will be discussed.

*Key words:* Ion guide. Ion trap. Ion cooling. Ion buncher. On-line mass spectrometry. Radioactive ion beams.

[1] corresponding author: Frank.Herfurth@cern.ch, phone/fax: +41 22 767 2780/8990

## 1 Introduction

The development of new techniques for the manipulation of radioactive ion beams is actively pursued by several groups worldwide. One of the main objectives is a better matching of the properties of the radioactive ion beams to the specific requirements of the experiments. Here ion trap techniques have started to play an increasingly important role, in particular for the accumulation, cooling, and bunching of these beams. Both, Penning traps [1] and radiofrequency multipole ion traps or guides [2] can fulfill this task. In addition, Penning traps offer high-resolution mass separation and can be used for beam purification [3]. Radiofrequency multipole ion guides have been employed in ion chemistry and molecular physics for many years [4,5]. Now they have gained increasing importance in the field of nuclear physics, where they are used for guiding charged nuclear reaction products from high-pressure gas cells into high-vacuum regions in order to form low-energy radioactive ion beams [6–9] or for enabling ultra-sensitive laser experiments on radioactive ions [10].

A rather new application is the use of radiofrequency multipole systems for the manipulation and improvement of radioactive ion beams as they are available from on-line mass separators. At the ISOLDE facility [11] at CERN, a beam accumulator, cooler, buncher, and emittance improver based on a linear radiofrequency quadrupole (RFQ) ion trap has been realized and used for on-line physics experiments. The system is installed at the Penning trap mass spectrometer ISOLTRAP [12]. Its task is the conversion of the continuous 60-keV ISOLDE ion beam into low-energy, low-emittance ion bunches that can be transferred with high efficiency into the mass spectrometer.

## 2 The ISOLTRAP facility

Figure 1 shows an overview of the layout of the ISOLTRAP Penning trap mass spectrometer together with the radiofrequency quadrupole ion beam buncher. The ISOLTRAP spectrometer itself consists of two Penning traps and has been described in detail in earlier publications [12,3]. Here only a short description of the tasks of the Penning traps and of the basic operation will be given.

Low-energy ion pulses delivered by the RFQ ion beam buncher are captured in the first Penning trap. The main task of this trap is the purification of the ion bunch from contaminating ions. A mass selective buffer gas cooling technique [13,14] is employed, which is based on the simultaneous application of a buffer gas and an RF excitation of the motion of the stored ions. This technique allows operation of the trap as an isobar separator with a resolving

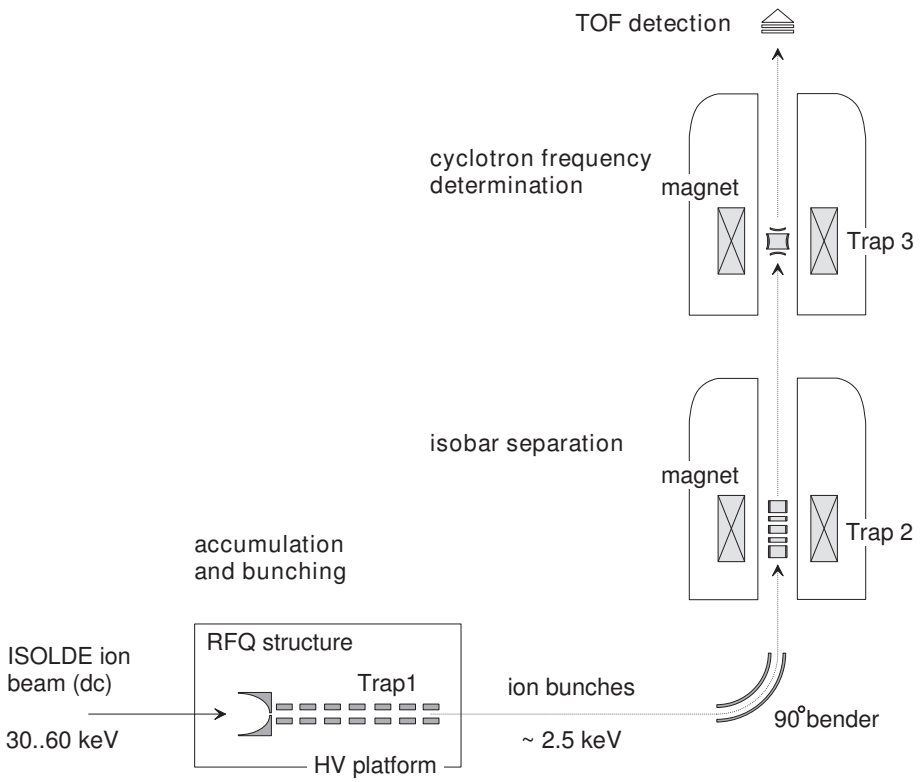


Fig. 1. Experimental setup of the ISOLTRAP Penning trap mass spectrometer and the linear RFQ ion beam buncher.

power of up to $R \approx 10^5$ for ions with mass number $A \approx 100$ [3].

The second trap is a high-precision trap [12,15] used for the mass measurement of the ions delivered by the first Penning trap. The mass measurement is carried out via a determination of the cyclotron frequency $\omega_c = \frac{q}{m}B$ of an ion with mass $m$ and charge $q$ in a magnetic field of known strength $B$. Using this technique, to date more than 150 isotopes have been investigated with a mass accuracy of $\delta m/m \approx 1 \cdot 10^{-7}$ (see for example [16,17]).

For the ISOLTRAP experiment (and any other ion trap experiment connected to an on-line mass separator), the most critical issue is the efficient transfer of the radioactive ion beam, which is typically of a few tens of keV in energy, into the ion trap. In an earlier version of ISOLTRAP, a stopping–reionization scheme was used in order to obtain a low-energy beam of radioactive ions. This approach limited the applicability of the Penning trap mass spectrometry to those elements that can be efficiently surface-ionized. Already several years ago, a development of an ion beam accumulator based on a Paul trap system was started. Such a system [2,18] was indeed realized and has been used successfully at the ISOLTRAP experiment [18]. However, it was found that the acceptance of the Paul trap system was not well matched to the ISOLDE beam emittance and that the ejection of the ions out of the system was very critical. The linear ion trap system to be discussed in this paper follows the

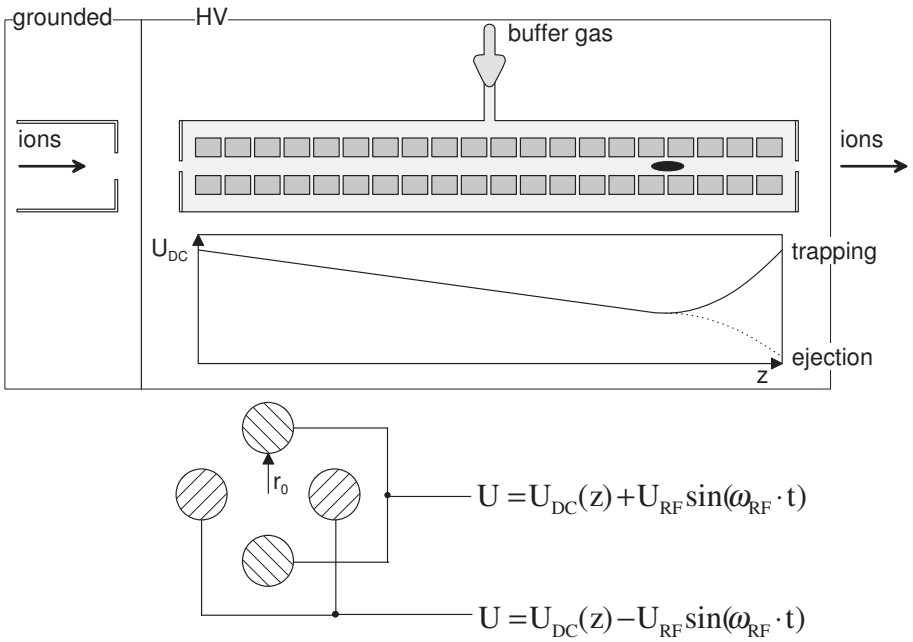


Fig. 2. Basic scheme of a radiofrequency ion beam cooler and buncher. The upper figure shows a schematic side view of such a system together with the potential along the symmetry axis. The lower figure shows the four rods and their supply with radiofrequency and DC voltages.

same concept as the earlier Paul trap system, but avoids these difficulties.

## 3 Principle of the ISOLTRAP ion beam cooler and buncher

The principle of the ISOLTRAP ion beam cooler and buncher is illustrated in Fig. 2. The 60-keV ISOLDE ion beam is electrostatically retarded to an energy of a few eV and injected into a linear radiofrequency quadrupole ion trap, which is filled with a buffer gas. The trap system consists of four segmented rods to which radiofrequency voltages are applied so as to obtain a transversely focusing force. The segmentation of the rods allows the creation of a DC electric field along the axis of the system. Ions entering the linear trap will lose transverse and longitudinal energy due to collisions with the buffer gas. They are finally accumulated in the potential well at the end of the system forming an ion bunch. By switching the potential of the last rod segments, as indicated in the figure, the ion bunch can be extracted. For a discussion of the principle of similar devices used as an ion guide see [19,20].

*3.1 Linear radiofrequency quadrupole ion traps*

The confinement of an ion in a linear RFQ trap as presented here is achieved by combining a static trapping potential $V_{\mathrm{DC}}$ along the axis of the system with a radial confinement. The latter results from the interaction of the trapped ion with a radiofrequency quadrupole field generated by the RF voltages applied to the quadrupole rods of the system.

The radial confinement in an exactly quadrupolar field can be described in terms of Mathieu equations [21,22], which also define the stability criteria of the motion. It is useful to consider the resulting motion as being that of a particle in a pseudopotential well [23] of depth $V_{\mathrm{RF}}$. While the electric field configuration of the linear trap produces motions that cannot be exactly described in terms of the Mathieu functions (due to the strong radial and azimuthal dependence of the axial field), it is still useful to consider the first-order solution of the motion as a linear superposition of the DC axial field potential and the RF quadrupole pseudopotential.

The pseudopotential is generated by radiofrequency voltages with amplitudes $\pm U_{\mathrm{RF}}$ and angular frequency $\omega_{\mathrm{RF}}$. As shown in Fig. 2, these voltages are applied with 180° phase difference to pairwise connected opposite elements of a quadrupole rod system. The separation between the surfaces of opposite electrodes is $2r_0$. The resulting pseudopotential is given by

$$V_{\mathrm{RF}}(r) = \frac{q \cdot U_{\mathrm{RF}}}{4r_0^2} r^2 \tag{1}$$

where

$$q = 4\frac{eU_{\mathrm{RF}}}{mr_0^2\omega_{\mathrm{RF}}^2} \tag{2}$$

is the relevant Mathieu parameter and $e$ and $m$ are the charge and mass of the stored ion. The solution of the Mathieu equation shows that the motion is stable as long as $q < 0.908$. In the radiofrequency field, the ion performs a micro-motion at the frequency $\omega_{\mathrm{RF}}$ of the field and a macro-motion that can be understood as an oscillation in the pseudopotential $V_{\mathrm{RF}}$. To a good approximation for $q < 0.6$, its oscillation frequency is

$$\omega_{\mathrm{m}} = \frac{q}{\sqrt{8}}\omega_{\mathrm{RF}} \quad . \tag{3}$$

As an example, a singly charged ion with mass number $A = 39$ in a four-rod structure with $r_0 = 6\,\mathrm{mm}$ operated with $\omega_{\mathrm{RF}} = 2\pi \cdot 1\,\mathrm{MHz}$, $U_{\mathrm{RF}} = 80\,\mathrm{V}$ will

experience a depth of the radial trapping potential of about 11 V in which it oscillates with $\omega_{\mathrm{m}} = 196\,\mathrm{kHz}$.

As illustrated in Fig. 2, the axial confinement is provided by applying DC voltages to the different segments of the rods in order to create a potential well along the trap axis. The minimum of the potential curve can be approximated by a parabola $V_{\mathrm{DC}}(r=0,z) = (U_{\mathrm{DC}}/z_0^2)\cdot z^2$ defined by the characteristic length $z_0$ and voltage $U_{\mathrm{DC}}$. Since $\triangle V_{\mathrm{DC}}(r,z) = 0$, the corresponding axisymmetric quadrupole potential is

$$V_{\mathrm{DC}}(r,z) = \frac{U_{\mathrm{DC}}}{z_0^2}\left(z^2 - \frac{r^2}{2}\right) \quad . \tag{4}$$

In the region where the DC potential along the trap axis has its minimum, the radial confinement due to the radiofrequency field is counteracted by the repelling radial part of the DC potential. The overall potential in the trap minimum then becomes

$$\bar{V}(r,z) = \frac{U_{\mathrm{DC}}}{z_0^2}z^2 + \left(\frac{q}{4}\frac{U_{\mathrm{RF}}}{r_0^2} - \frac{U_{\mathrm{DC}}}{2z_0^2}\right)r^2 \quad . \tag{5}$$

With the parameters used above and $U_{\mathrm{DC}}/z_0^2 = 10\,\mathrm{V/cm^2}$, the radial trapping potential well is reduced by about 1.8 V compared to the RF-only case. From Eq. 5 the condition

$$U_{\mathrm{RF,min}} = r_0^2 \cdot \omega_{\mathrm{RF}}\sqrt{\frac{m}{e}\frac{U_{\mathrm{DC}}}{2z_0^2}} \tag{6}$$

can be derived for the minimum RF voltage required for three-dimensional ion trapping.

### *3.2 Buffer gas cooling*

After the ions have entered the linear radiofrequency quadrupole, they interact with the buffer gas. The ions are elastically scattered at the buffer-gas atoms transferring part of their energy to them. Thus, the motion of the ions is damped until they finally come into thermal equilibrium with the buffer gas in the minimum of the trapping potential.

To study the overall cooling process, it is sufficient to describe the action of the gas as that of a viscous force. However, for an understanding of ion loss mechanisms and final ion temperatures, a microscopic modelling of the deceleration and cooling process including the radiofrequency field is required.

Various calculations of both kinds have been carried out for the system presented here. In the following the most basic aspects of buffer gas cooling in such a system will be discussed.

For low ion energies (less than a few eV), the damping of the ion motion is dominated by the long-range interaction of the ion with buffer gas atoms, polarized by this ion. This interaction results in an average damping force

$$\vec{F} = -\delta \cdot m \cdot \vec{v} \quad , \tag{7}$$

where $m$ and $v$ are the mass and the velocity of the ion. The damping coefficient

$$\delta = \frac{e}{m}\frac{1}{\mu}\frac{p/p_{\mathrm{N}}}{T/T_{\mathrm{N}}} \tag{8}$$

is proportional to the gas pressure $p$ (in fractions of the normal pressure $p_{\mathrm{N}}$) and inversely proportional to the temperature $T$ (in fractions of the normal temperature $T_{\mathrm{N}}$) and the reduced ion mobility $\mu$ [24], which for low kinetic energies of the ions is constant for a given ion species and type of buffer gas. For kinetic energies $> 1\,\mathrm{eV}$ the ion mobility decreases (see discussion in [19]). For the purpose of this paper it is sufficient to take the constant low-energy values as an upper limit for the ion mobility.

Figure 3 illustrates the cooling and accumulation process in a linear trap with an axial potential as shown in Fig. 2. The simulation has been performed for a $^{39}\mathrm{K}^+$ ion entering the system with an initial kinetic energy of $E_{\mathrm{kin}} = 10\,\mathrm{eV}$. The axial potential well depth is $V_{\mathrm{z0}} = 50\,\mathrm{V}$ and the trap has a total length of $L = 1\,\mathrm{m}$ with the potential minimum at $l_0 = 0.8\,\mathrm{m}$. A helium buffer gas pressure of $p_{\mathrm{He}} = 10^{-2}\,\mathrm{mbar}$ has been used. With an ion mobility $\mu(\mathrm{K}^+ - \mathrm{He}) = 2.15 \cdot 10^{-3}\,\mathrm{m^2/Vs}$, the damping constant reaches a value of $\delta = 11500\,\mathrm{s}^{-1}$. As can be seen in Fig. 3(a) and (b), both the axial and the radial oscillation amplitude of the ion are damped very quickly. Even more illustrative is Fig. 3(c) which shows the total energy of the ion as a function of the axial position. Already during its first oscillation in the system the ion loses more than 50 % of its initial total energy. The equilibrium with the buffer-gas temperature is reached within about 1 ms.

The viscous damping approach presented above is valid at low velocity for ions with masses much heavier than the mass of the buffer gas atoms. Figure 4 illustrates the limits of this approach. A comparison of the ion motion in the first (linear potential) part of the quadrupole system is shown, as calculated under the assumption of viscous damping and in a full Monte-Carlo calculation. In this calculation the trajectories of several thousand ions have been investigated using realistic interaction potentials for the collision of the

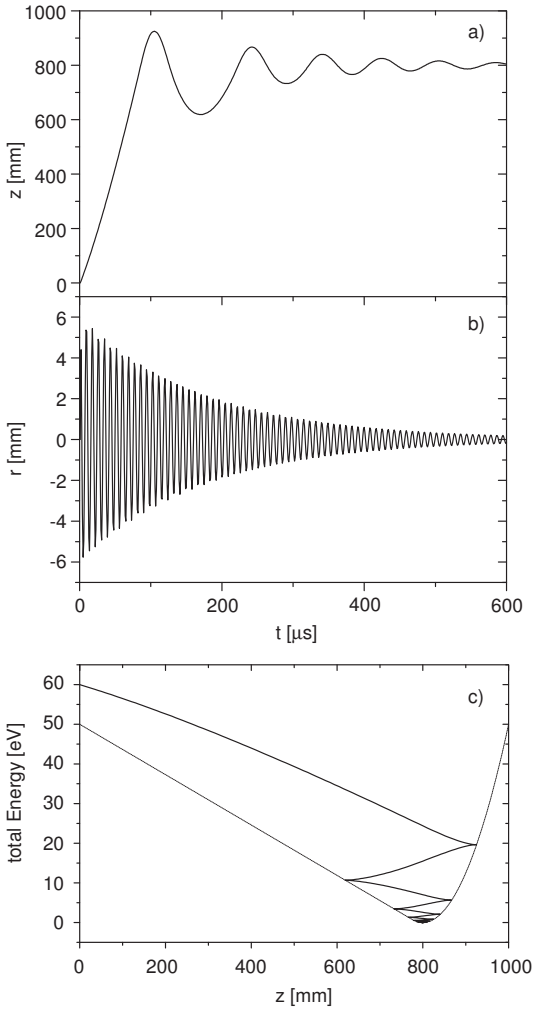


Fig. 3. Simulation of the accumulation and cooling process in a linear RFQ trap: a) the axial oscillation as a function of time, b) the radial oscillation as a function of time, and c) the total axial energy as a function of the axial position (shown together with the axial potential).

ions with the buffer-gas atoms (details of this microscopic calculation will be discussed in an upcoming publication [25]). In the case of Cs ions in He, the validity of the viscous damping description is nicely confirmed, and even for $Cs^+$ in Ar, good agreement is obtained in the time average. However, in the case of $K^+$ in Kr, the motion becomes unstable very quickly and the ion is radially ejected out of the system. The reason is that the micro-motion of an ion colliding with a heavier atom can make a phase jump with respect to the radiofrequency which leads to an increase of the kinetic energy. This process is called RF-heating. In the case of light ions and a heavy gas, it is the predominant cause of ion loss from RFQ traps.

In order to determine the properties of ion bunches extracted from the trap, the final spatial distribution of the trapped and cooled ions is of interest. As

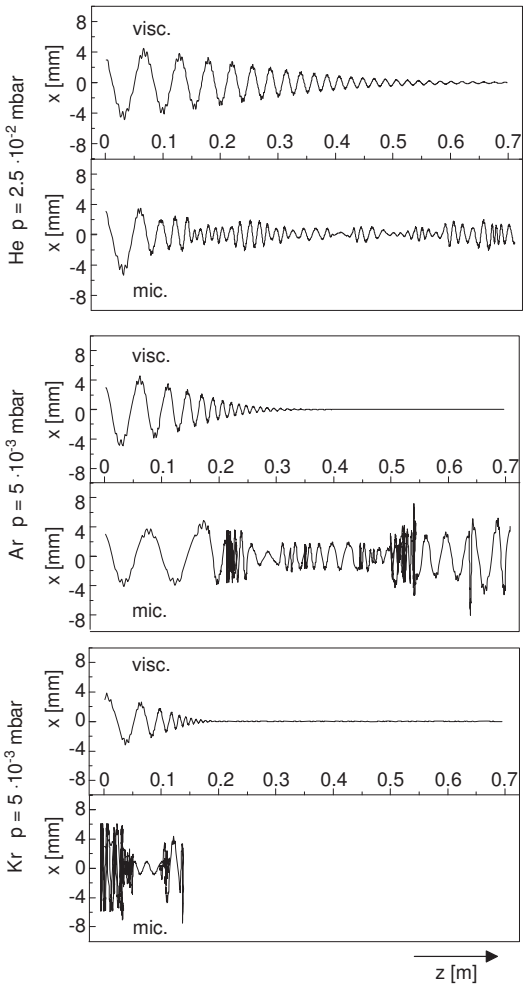


Fig. 4. Comparison of ion damping in a linear cooler as obtained by calculations based on a viscous damping approach (**visc**) and a microscopic description (**mic**). Shown is the radial position of the ions as a function of their axial position. The calculations have been performed for $K^+$ in He, Ar, and Kr at different pressures.

a first approach we take the form of the overall potential in the trap center from Eq. 5 and the parameters as used above and assume that the ions reach a final temperature $T = 300\,\mathrm{K}$ equal to that of the buffer gas. Assuming Boltzmann distributions, we obtain axial and transverse distributions as shown as solid curves in Fig. 5 for $Cs^+$ ions. The points are the result of a microscopic calculation. It can be seen that the oscillating electrical field and the collisions with the gas have only a very small effect on the ion distribution for $Cs^+$ in Ar but a significant one for $Cs^+$ in Xe. Practically no effect is seen for $Cs^+$ in He, not shown in the figure here.

### *3.3 Ion injection and extraction*

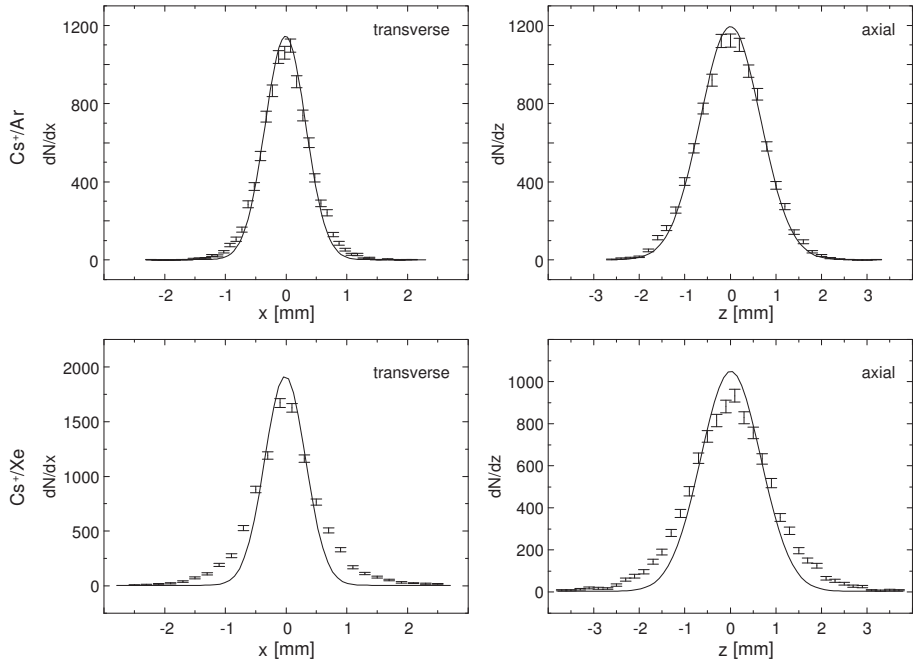


Fig. 5. Transverse and axial amplitude distribution of Cs ions in the potential minimum of the linear ion trap. The solid curves show distributions for an ion cloud temperature of 300 K in the total static (pseudo)-potential. The points are the result of a microscopic calculation taking the RF field and ion-atom collisions into account.

### *3.3.1 Deceleration and injection*

In order to stop an energetic ion beam in the linear ion trap by gas collisions, first the beam has to be decelerated to low energies (in the order of 10 eV). This can be accomplished by placing the whole ion trap on a potential slightly below the corresponding ion beam energy. With reduction of energy the divergence of the beam increases. Therefore, it depends on the original emittance of the ion beam how far the energy of the beam can be reduced by electrostatic means. For example, an ion beam of $E_0 = 60\,\mathrm{keV}$ with an emittance of $\epsilon = 35\,\pi\,\mathrm{mm\,mrad}$ that is decelerated to $E_1 = 20\,\mathrm{eV}$ and focused to fit through a 5-mm-diameter opening has a maximum divergence of $\theta \approx 45^o$ and a maximum transverse energy of about 10 eV. Whether such a beam can be injected into a linear trap without losses depends on the acceptance of the system. The latter is determined by the transverse dimensions and the transverse focusing force inside the trap.

For the ion beam buncher discussed here, a number of injection calculations have been performed in order to determine the acceptance of the system. As an example, Fig. 6 shows a comparison of the transverse acceptance of the ISOLTRAP ion beam buncher and the transverse emittance of the ISOLDE ion beam, both at beam energies of 30 keV. The diagrams are calculated at a position 140 mm upstream from the 6-mm hole of the retardation electrode.

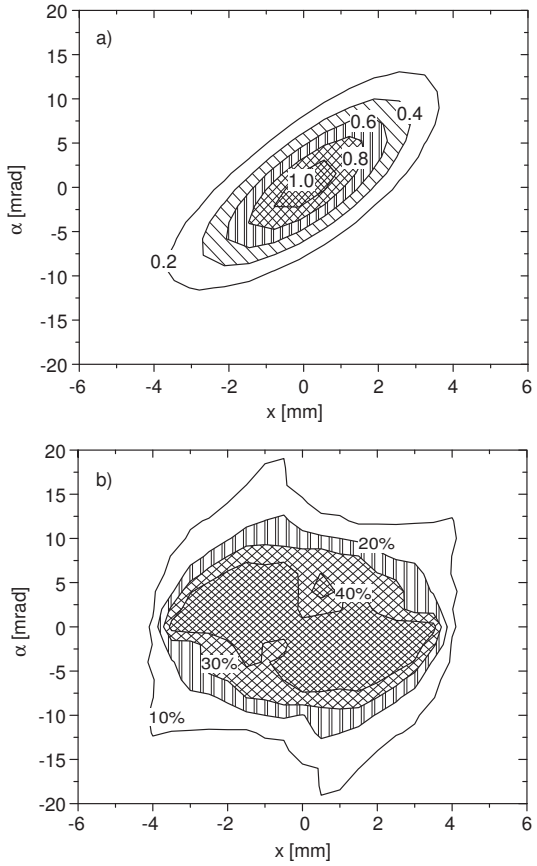


Fig. 6. a): emittance diagram of the ISOLDE ion beam. Shown is the ISOLDE beam intensity (in arbitrary units) as a function of beam displacement $x$ and angle $\alpha$. b): acceptance diagram of the ISOLTRAP ion cooler and buncher for $x$ and $\alpha$. Shown is the probability of successful ion injection, obtained by averaging over the results of the beam parameters $y$ and $\beta$ and all RF phases.

The emittance diagram was obtained from beam transport calculations (GIOSP [26]) of the ISOLDE beam from the ion source to the apparatus. The focusing parameters of ISOLDE beam line elements were varied until maximum overlap with the buncher acceptance was obtained. For the acceptance diagram, a Monte-Carlo simulation for the ion injection into the buncher was performed (for the RFQ parameters see Table 2). An ion was considered to be confined when it passed the first 200 mm of the quadrupole rod system without hitting an electrode. The calculation was repeated for various phases of the radiofrequency field. For each $x$ and $\alpha$ value an average of the result was taken including the beam dimensions $x$ and $\beta$. The result is the acceptance diagram shown in Fig. 6(b). From this acceptance and the ISOLDE beam emittance a value of $\epsilon_{\mathrm{calc}} \approx 35\,\%$ is obtained for the theoretical capture efficiency.

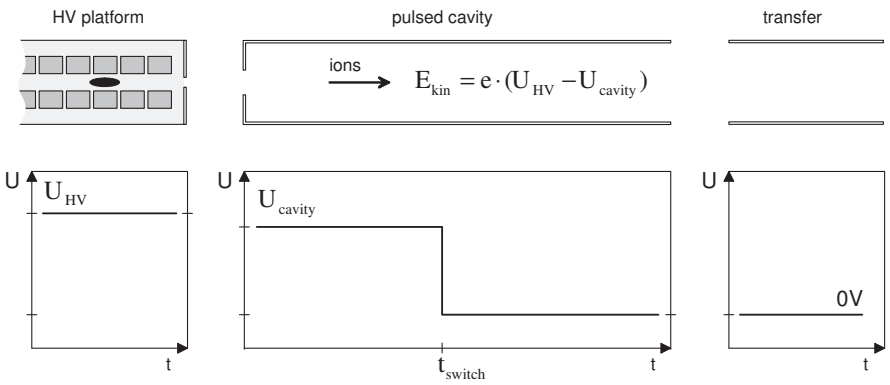


Fig. 7. Principle of creating variable energy ion pulses by employing a pulsed cavity

### *3.3.2 Extraction and acceleration*

When the ions have been accumulated in the trap potential minimum, they can be extracted by switching the potential as indicated in Fig. 2. With appropriate voltages applied to the electrodes, ion pulses not longer than a few micro seconds can be generated. The beam properties of the extracted ion pulses depend on the temperature and spatial distribution of the ion cloud. The time structure depends in addition on the shape of the potential used to extract the ions. If no further measures are taken, the ion pulse leaving the trap at the potential of the HV platform will be accelerated towards ground potential and once again reach the energy of the injected ion beam. For the transfer into the ISOLTRAP Penning traps, low-energy ($\approx 2.5\,keV$) ion pulses are required.

An elegant way to modify the potential energy of an ion pulse is to have the ions enter a pulsed cavity. The principle is illustrated in Fig. 7. After having left the linear ion trap at a potential $U_{\mathrm{HV}}$ the ion pulse is accelerated towards a cavity at a potential $U_{\mathrm{cavity}}$ to gain a kinetic energy $E_{\mathrm{kin}} = e \cdot (U_{\mathrm{HV}} - U_{\mathrm{cavity}})$. When the ion pulse reaches the field-free region inside the cavity, the latter is switched to ground potential and the ions leave it without any further change of their kinetic energy.

## 4 The experimental setup

Figure 8 shows the setup of the ISOLTRAP ion beam cooler and buncher. On one side the system is connected to the ISOLDE beam line system and on the other side to the ion beam transport system of ISOLTRAP. A 60-keV test ion source and a beam switchyard (not shown in the figure) are installed upstream in the ISOLDE beam line in order to allow test measurements without the ISOLDE ion beam. Beam intensities and profiles can be measured with a needle beam scanner and a Faraday cup in front of the ion beam buncher. Most of the relevant parts of the cooler and buncher, including the electronics

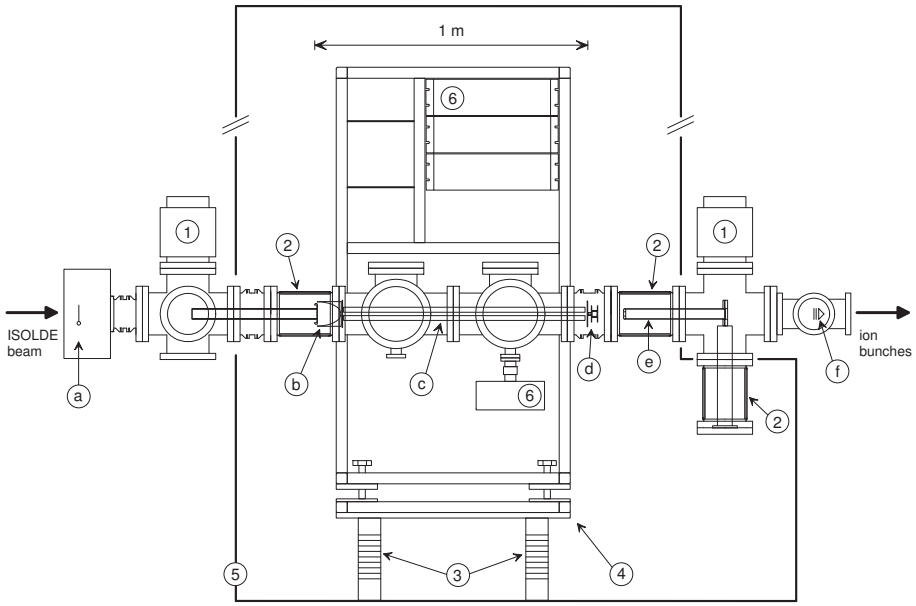


Fig. 8. Experimental setup of the ISOLTRAP ion beam cooler and buncher. The main components are: (1) turbo-molecular pump, (2) insulator, (3) insulating support, (4) HV platform, (5) grounded cage, (6) DC and RF supplies, (a) beam scanner and Faraday cup, (b) deceleration section, (c) linear ion trap, (d) extraction section, (e) pulsed cavity, (f) MCP detector.

and the gas inlet system, are placed on a 60-kV high-voltage platform in a high-voltage cage. Ceramic insulators separate the vacuum system on the HV platform from the beam lines on ground potential. Efficient pumping is achieved by turbo-molecular pumps at ground potential placed close to the

Table 1
Dimensions of the ISOLTRAP ion beam buncher

| Element | Dimension [mm] |
|---|---|
| diameter of injection hole | 6 |
| diameter of extraction hole | 6 |
| distance between opposite rods ($2 \cdot r_0$) | 12 |
| diameter of rod segments | 18 |
| total length of quadrupole rods | 881.5 |
| length of rod segments | |
| # 1, 2 | 20.5 |
| # 3 – 19 | 41.5 |
| # 20 | 20.5 |
| # 21 | 41.5 |
| # 22 – 25 | 10.0 |
| # 26 | 20.5 |
| length of pulsed cavity | 380 |

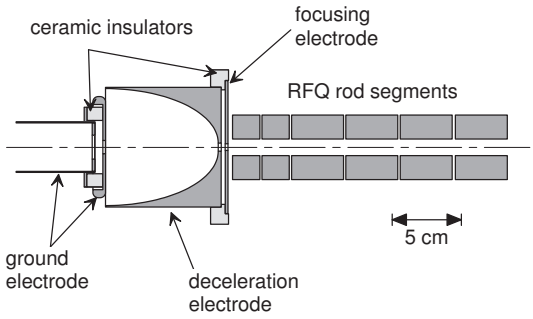


Fig. 9. Ion optical elements for the deceleration of the 60 keV ion beam and first part of the linear ion trap.

insulators.

The ion-optical elements of the cooler and buncher can be grouped into three functional sections. In the first section the deceleration of the ISOLDE ion beam takes place, the second section is the linear ion trap, and in the third section the extracted ion bunches are accelerated to the desired transport energy. All electrodes are made of stainless steel. Alumina or glass ceramic (Macor) are used for insulating parts. The electrical connections to the ion-optical elements are made via UHV multi-pin feedthroughs and Kapton-insulated wires. Table 1 summarizes some important mechanical parameters of the system which will be discussed below in more detail.

### *4.1 The deceleration and injection section*

Figure 9 shows the design of the deceleration electrode system and its connection to the linear ion trap system discussed below. This deceleration electrode system is the copy of a prototype described in more detail in [20]. The ISOLDE ion beam enters through the ground electrode which is equipped with an insulated diaphragm for current measurements. The shape of the deceleration electrode is designed to focus the beam through the 6-mm opening at its end. An additional electrode and the first segments of the four-rod structure are used to obtain the final retardation and to focus the beam towards the axis of the system.

For the presented cooler and buncher ion optical simulations were performed so as to determine the optimal position of the ground electrode with respect to the deceleration electrode and to get a set of voltages that give the best injection efficiency into the trap system. These voltages were used as start values for the experimental optimization. A set of typical voltages for the deceleration section are listed in Table 2 below together with parameters for the other sections.

Figure 10 shows a photograph of the assembled electrode system of the linear ion trap with the deceleration electrode mounted. Figure 11 shows a detailed view of a part of a rod and how the cylindrical electrode segments are mounted together. The quadrupole rods have a total length of 881.5 mm. Each rod con-

Fig. 10. Photograph of the assembled four-rod electrode system of the ISOLTRAP ion beam cooler and buncher and the mounted deceleration electrode.

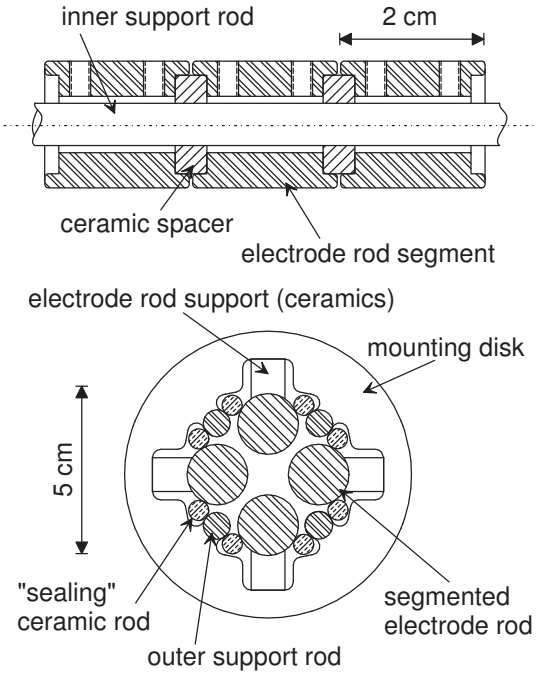


Fig. 11. Detail of the rod structure. The segments are insulated from each other by ceramic spacers. The four rods are mounted to disks as shown in the lower part.

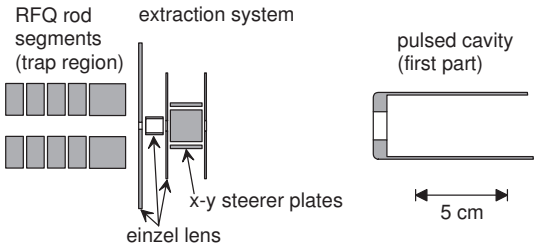


Fig. 12. Exit side of the linear trap with extraction lens, x-y steerers and a pulsed cavity

sists of 26 segments. All electrodes have a diameter of 18 mm. They are aligned by four inner support rods with ceramic insulators in-between, separating the electrodes by 0.5 mm axially. The quadrupole rods themselves are mounted via ceramic supports to four mounting disks as shown in the lower part of the fig. 11. The inner distance between opposite quadrupole rods is $2r_0 = 12$ mm. The holding disks are kept at fixed distances by the four outer support rods. Additional ceramic rods are provided to "seal" the system. This is to maximize the gas pressure inside the trap while minimizing the pumping requirements of the whole system. Electrode segments of various lengths are used (see Table 1). The shorter segments at the entrance of the trap allow to set up an axial potential gradient for retardation and focusing of the incoming ions as discussed above. In the part of the trap where the potential decreases slowly and linearly, longer segments are sufficient. A high segmentation is again required in the region where the ions are finally accumulated and ejected.

### *4.3 The extraction section and the pulsed cavity*

Figure 12 shows the extraction optics of the buncher and the pulsed cavity. The extraction hole has a diameter of 6 mm. The extraction optics consists of an einzel lens formed by a cylindrical electrode between two diaphragms and a set of x-y steerers. The purpose of this arrangement is to adapt the divergence of the extracted ion bunch to the ion optics downstream and to allow adjustments of the ion-flight direction.

At a distance of 90 mm downstream from the extraction optics, the ions enter the pulsed cavity, which is only partly shown in the figure. The cavity is designed to shield the ion pulse from external fields and has a total length of 380 mm. This is larger than the expected length of a pulse of ions with mass number $A > 20$ that is injected into the cavity with an kinetic energy of 2 to 3 keV. In Fig. 8 it can be seen that the pulsed cavity is fixed to a support directly mounted on an insulated flange perpendicular to the beam axis.

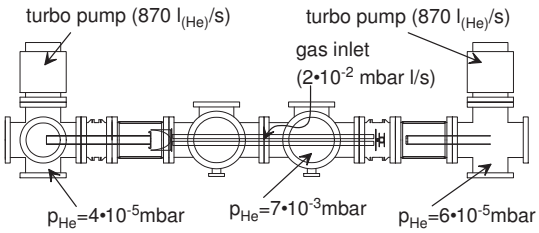


Fig. 13. Schematic of the vacuum system of the ISOLTRAP ion beam cooler and buncher. Gas flow value (valve controller reading), pumping speeds (for He), and measured pressures values (He-corrected) are shown.

### *4.4 Vacuum system and gas supply*

Figure 13 gives a schematic overview of the vacuum and gas inlet system. The vacuum system that houses the ion-optical parts discussed above consists of several vacuum chambers mostly of CF 150 size. Two magnetic-bearing turbo-molecular pumps (Pfeiffer TMU 1000MC) with a pumping speed of 870 l/s for helium are connected on both sides of the system. These pumps are backed by one 40 $m^3$/h roughing pump. Differential pumping is accomplished by diaphragms at the entrance and exit side in order to reduce the gas flow out of the trapping region. The trap is mainly pumped via the entrance and exit holes for the ions. The buffer-gas inlet is via a needle valve connected to a pressure controller (Balzers EVR 116 + RVC 200). Inside the vacuum chamber, a thin stainless steel tube guides the gas into the central region of the RFQ structure. A full-range pressure gauge (Balzers PKR 250) is connected to the vacuum chamber on the HV platform. Its reading is used as the input for the pressure controller. The pressure value measured with the gauge is of course lower than the pressure inside the structure. From gas flow simulations, it is expected that the gauge gives a reading which is about a factor of 10 lower than the actual pressure inside the center of the structure [2].

A reasonable working pressure inside the RF-structure is $p_{\mathrm{He}} \approx 10^{-2}$ mbar. With the resulting gas load, care has to be taken about possible discharge processes in the system. A critical point is the region where the ground injection electrode is close to the deceleration electrode (Fig. 9) with a gap of 5 mm and a potential difference of up to 60 kV. One has to make sure that at this gap a pressure regime is reached, where the discharge probability is minimized. The Paschen curve [27] for helium gives a maximum pressure of the order of $10^{-5}$ mbar. Gas flow calculations have confirmed that such values can be reached with the applied pumping speed, the entrance and exit openings of the linear trap, the desired inside pressure, and the required gas flow. The experimentally measured pressures are given in Fig. 13.

[2] In this paper, the values given for the measured pressure are the vacuum gauge readings corrected for the gas-specific factor.

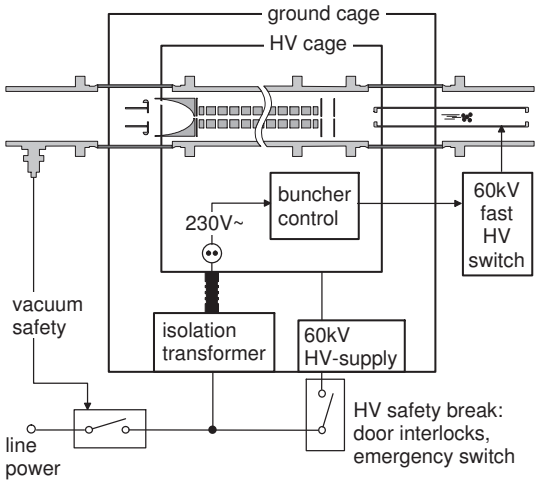


Fig. 14. Line power and HV supply for the high-voltage platform. Also shown are the safety interlocks that cut the high voltage in the event of too high pressure and allow safe access to the cage.

Another point of concern are gas impurities in the system which can give rise to charge exchange and loss of ions. Such effects have been seen in the start-up of the system when ions like argon were injected into the ion beam cooler and buncher. Meanwhile, this has been cured by baking the whole system. Furthermore, pellets of non-evaporable getter material (SAES St 172 type) have been installed in the gas inlet line of the buncher for gas purification.

### *4.5 Electronics and control system*

#### *4.5.1 The high-voltage system*

Figure 14 shows schematically the high-voltage and the line power supply for the high-voltage platform. An oil-free 2-kW isolation transformer is used to provide line power to the platform. The platform potential is provided by a remote-controllable power supply (FUG HCN 140M-65000) with a maximum voltage of 65 kV and a short- and long-term voltage stability of $10^{-5}$. This power supply is connected to the secondary windings of the transformer via a 5.6-k$\Omega$ current-limiting resistor. Varistors across the secondary winding of the isolation transformer protect the electronic equipment on the high-voltage platform from high-voltage transients caused by occasional sparkovers.

Figure 15 shows the circuit used for the switching of the potential of the cavity. A fast high-voltage transistor switch (Behlke HTS 650) discharges the cavity with a fall-time $t_\mathrm{f} = 220\,\mathrm{ns}$. After a constant on-time of $60\,\mu\mathrm{s}$ the switch opens again, allowing the cavity to be charged again to high voltage with a rise-time $t_\mathrm{r} = 22\,\mathrm{ms}$. Due to the internal resistance of the high voltage switch, the cavity can only be discharged to ground when a negative bias voltage of

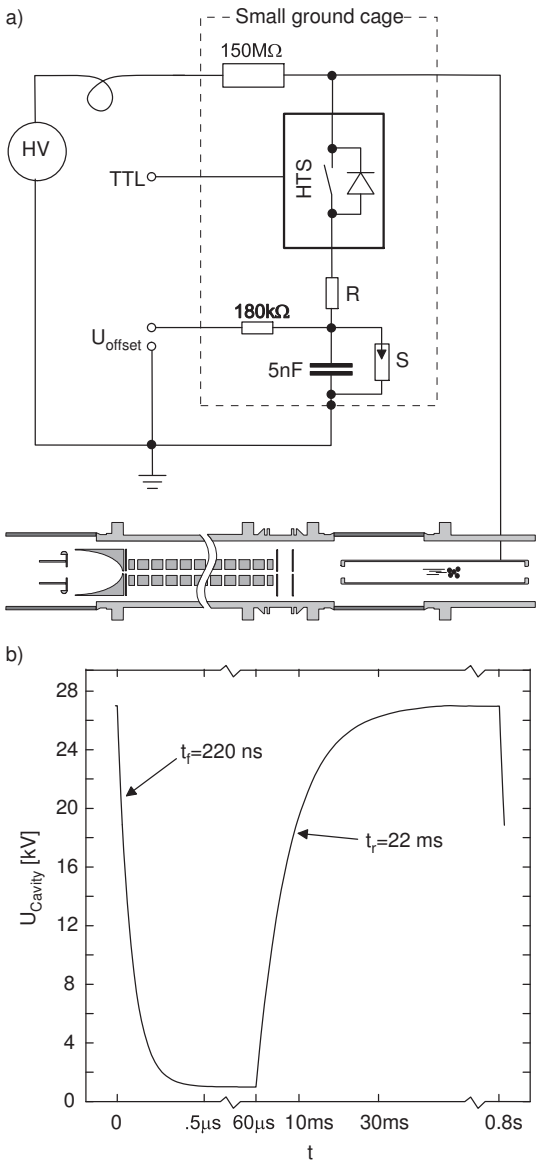


Fig. 15. Circuit used for the fast switching of the pulsed cavity from a potential of $\leq$60 kV to ground potential (a). Measured voltage for a switching from $\approx$30 keV to ground as a function of time (b). HV: high-voltage power supply; HTS: high-voltage transistor switch; $U_{\mathrm{offset}}$: compensating voltage for the voltage drop over the internal resistance of the HTS; S: spark gap. The times $t_{\mathrm{f}}$ (fall-time) and $t_{\mathrm{r}}$ (rise-time) are the times needed for the signal to change between 10 and 90% of its maximum strength.

several hundred volts is applied to the point marked $U_{\mathrm{offset}}$ (a typical value is $\approx$ 500 V). A spark gap S serves to protect the low-voltage side of the circuit.

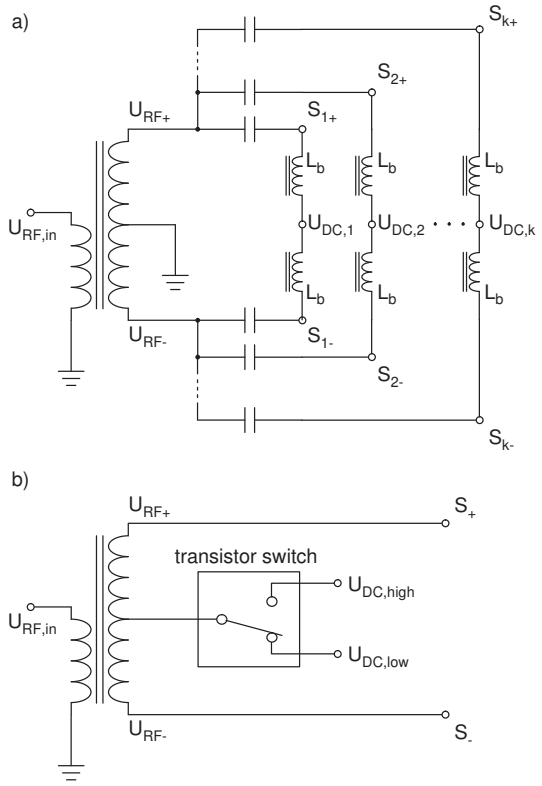


Fig. 16. Principle of the electronic circuits used to provide the different segments $S_{k\pm}$ of the four rods with DC ($U_{\mathrm{DC},k}$) and RF ($U_{\mathrm{RF}\pm}$) voltages. a) circuit for those electrodes which require RF and static DC voltages; b) circuit for those electrodes which require RF and switched DC voltages.

### *4.5.2 Radiofrequency and DC supplies for the buncher*

The RF voltage for the radial pseudopotential has to be applied to all segments of the system but with a phase shift of 180° between segments of neighboring rods. The DC potentials are applied in two different modes, depending on whether the element is used for a static potential or whether the potential is dynamically switched within less than one microsecond.

Two different types of circuits are used. The circuit shown in Fig. 16(a) is used for all elements where a static DC voltage is required. The RF voltage $U_{\mathrm{RF,in}}$ is provided by a function generator (Stanford Research DS 345) after amplification by a 200-W radiofrequency amplifier (ENI 240L) and fed into a transformer. The secondary winding has a grounded center tap in order to generate two symmetrical radiofrequency signals $U_{\mathrm{RF}\pm}$ of opposite sign. These RF voltages are added via capacitors $C = 10\,\mathrm{nF}$ to the DC voltages $U_{\mathrm{DC},i}$ ($i = 1 \ldots k$) in order to obtain a combined RF/DC signal which applied to the different pairs of electrodes $S_{i\pm}$ ($i = 1 \ldots k$). Two inductances $L_\mathrm{b} = 3.9\,\mathrm{mH}$ protect each DC feeding point from the two RF signals. The DC voltages are provided by 0 to 500-V power supply modules (Brandenburg). The voltage series required for the generation of the linear potential slope (see Fig. 2) is

obtained via a resistive voltage divider chain fed by two of the DC power supply modules. The most critical electrodes closest to the injection side of the buncher and those in the trapping region have separate voltage supplies. The inductance of the transformer and the capacitances have been matched to the capacitance of the electrodes in order to obtain a maximum RF voltage at a frequency of $\nu \approx 1$ MHz. An amplitude $U_{\mathrm{RF}} \approx 125$ V is reached with about 40 W RF power.

For the extraction of the ions from the buncher it is necessary to switch the potential of the last segments of the linear trap very quickly. Therefore, the relevant segments are supplied with a circuit as shown in Fig. 16(b). The DC voltage from the DC modules is sent to the center tap of the transformer via a fast transistor switch. With this system, a fall-time of 0.5 $\mu$s is obtained.

A number of additional power supplies is used for the voltages of the deceleration and focusing electrode (see Fig. 9) and the extraction optics (see Fig. 12). The high voltage $U_{\mathrm{cavity}}$ for the pulsed cavity (see Fig. 15) is also provided from the HV platform.

### *4.5.3 The control system*

Figure 17 shows the layout of those parts of the control system relevant for the operation of the cooler and buncher. Since most of the electronics is installed on the HV platform, remote control of the system is mandatory. Three different optical links provide the communication between the VME-based computer system of the ISOLTRAP spectrometer and the electronics on the HV-platform. A GPIB link (National Instruments GPIB-140) is used to control the function generator for the radiofrequency signal and to read out a pico-amperemeter. A field bus system (Profibus) equipped with DACs and ADCs is used for analog programming and monitoring a total of 28 voltage supplies. It also serves for programming the pressure regulation system. A fast TTL link (Harting) is used to provide the trigger for the fast voltage switching required for the ion extraction from the buncher.

### *4.5.4 Diagnostics*

Several tools are available for the optimization and diagnosis of the performance of the ion beam buncher. The ISOLDE beam scanner and movable Faraday-cup in front of the buncher allow the measurement of profile and current of beams from both ISOLDE and the test ion source. In order to optimize the injection of the 60-keV ion beam into the buncher, it is important to perform a beam current measurement on the high-voltage platform. For this purpose a pico-amperemeter (Keithley 485) is installed on the platform which can be connected to any of the buncher electrodes. On the ejection side

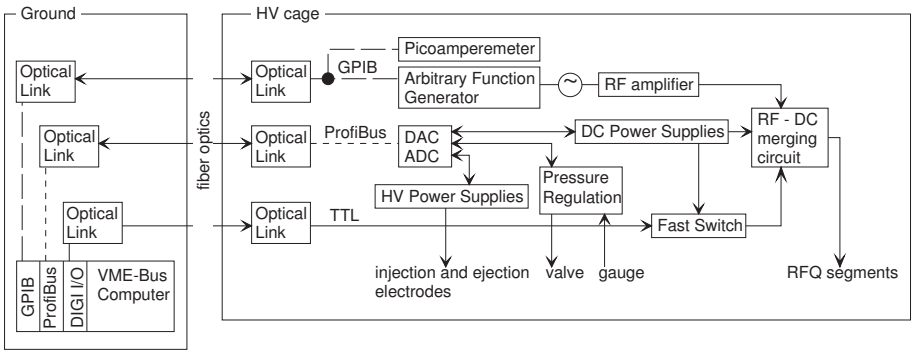


Fig. 17. Layout of the control system of the ISOLTRAP buncher. The electronics on the HV platform is controlled via three optical links.

another Faraday cup and a micro-channel plate (MCP) detector are available. This detector consists of 2 MCP's with 18 mm active area mounted in a Chevron arrangement. No electron repelling grid is used (see discussion in section 6.2). This MCP detector has been used for most of the test measurements reported below. More MCP detectors are available further downstream for the tuning of the ion beam transport to the Penning trap system. In addition, a beam viewing system is available which can be installed behind the 90° vertical deflector (see fig. 1) to obtain the spatial distribution of the ion beam. This system (Colutron BVS-2), which is mounted on a flange with a viewport, consists of an MCP with a phosphor screen behind it. The fluorescent light from the phosphor screen originated by the secondary electrons of the MCP after ion impact, can be viewed through this window with a CCD camera. When this detector is used the deflector electrode system is removed from its vacuum chamber in order to allow the ions to pass through.

## 5 Operation

Table 2 gives a typical set of operating parameters for ions with mass number close to $A = 39$ and $A = 133$. The ions enter the linear trap with an energy of 20 eV after retardation. The value given for the buffer gas pressure value is the (helium-corrected) vacuum gauge reading. As discussed above the pressure inside the linear trap is estimated to be a factor of 10 higher. Depending on the delivered ion beam current, the ions are accumulated for a period $T_{\mathrm{accu}} = 0.01 \ldots 1000\,\mathrm{ms}$. Then the ions are allowed to complete their cooling into the trap potential minimum for an additional period $T_{\mathrm{cool}} = 2\,\mathrm{ms}$ before they are ejected. The timing of the switching of the cavity is adapted to the mass-dependent time of flight of the ions. For a 2.65-keV extraction and an $A = 40$ ion, $t_{\mathrm{switch}} = 12\,\mu\mathrm{s}$. The system has been tested with repetition rates up to 5 Hz. In general, repetition rates of $\approx$1 Hz are used for the mass measurements.

Table 2
Typical operating parameters of the cooler and buncher for ions in the mass ranges $A \approx 39$ and $A \approx 133$.

| Parameter | | Value | |
|---|---|---|---|
| helium pressure (at gauge position) $p_{\mathrm{He}}$ | | $6 \cdot 10^{-3}$ | mbar |
| RF frequency $\nu_{\mathrm{RF}} = \omega_{\mathrm{RF}}/2\pi$ | | 970 | kHz |
| RF amplitude $U_{\mathrm{RF}}$ | for $A \approx 133$ | 135 | V |
| | for $A \approx 39$ | 97 | V |
| cooling time $T_{\mathrm{cool}}$ | for $A \approx 133$ | 10 | ms |
| | for $A \approx 39$ | 2 | ms |
| cage voltage $U_{\mathrm{HV}}$ | | 30 | kV |
| electrode voltages $U_{\mathrm{elec}}$ relative to the cage voltage $U_{\mathrm{HV}}$: | | | |
| deceleration electrode | | –1350 | V |
| focusing electrode | | –230 | V |
| quadrupole rod segment | # 1 | –60 | V |
| | # 2 | –40 | V |
| | # 3 | –25 | V |
| | # 4 to # 22 | –10 to –20 | V |
| | # 23 (accumulation) | –24 | V |
| | # 23 (ejection) | +2 | V |
| | # 24, # 25 | –29 | V |
| | # 26 (accumulation) | 0 | V |
| | # 26 (ejection) | –55 | V |
| plates of the extraction system | | –420 | V |
| einzel lens | | –55 | V |
| pulsed cavity ($U_{\mathrm{offset}} = -500$ V, see Fig. 15) | | –2650 | V |

## 6 Performance of the ISOLTRAP ion beam buncher

A number of systematic investigations have been performed with the buncher in order to characterize its performance and to compare the results with simulations. For these measurements, both ions from ISOLDE and from the test ion source have been used.

### *6.1 Injection, capture, and ejection*

#### *6.1.1 Ion energy*

A critical parameter for the injection and capture of the ions into the buncher is the energy of the ions when they enter the system. This energy is determined

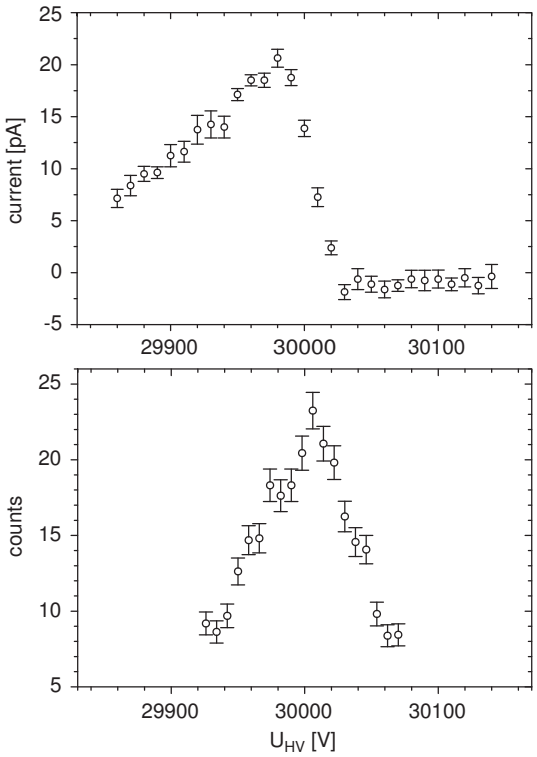


Fig. 18. Current of $^{132}Xe^{+}$ ions guided through the RFQ (top) and number of accumulated and ejected ions in bunching mode (bottom) as a function of the voltage $U_{\mathrm{HV}}$ of the HV platform.

by the potential of the linear trap on the HV platform with respect to the initial ion beam energy. If the potential is too high, then the ions are not able to enter the system. If it is too low, then the energy loss in the gas is not sufficient to prevent the ions from leaving the system on the exit side or to be stopped on the extraction diaphragm.

In order to optimize the injection and the platform potential, two kinds of measurements are performed. In the first case, all electrodes of the extraction system (see Fig. 12) are connected together for a direct current measurement. Radiofrequency and DC potentials are applied to the segmented rods as given in Tab. 2 for the ejection mode. No buffer-gas is used.

In Fig. 18 (top) the result of such a measurement is shown for a 30-keV $^{132}Xe^{+}$-ion beam as a function of the potential of the HV platform. At the ion beam energy of 30 keV a maximum in the transmission is observed. Increasing the potential from 30 000 V to 30 030 V gives a sharp drop in transmission. At a potential larger than 30 030 V no ions are transmitted. For potentials lower than 30 kV and correspondingly higher ion beam energy in the system, the transmission decreases gradually. This can be understood since the focusing of the ion optics in the injection part was optimized for a beam entering the cooler and buncher at about 20 eV kinetic energy.

This transmission mode of operation is particularly useful for a fast tuning of the beam injection into the cooler and buncher. The platform potential is set to the value giving maximum transmission and then the current at the end of the structure is monitored as a function of focusing and steering voltages applied to ion optical elements in the ISOLDE beam line.

For fine tuning of the injection (in particular of the platform potential), the full accumulation-ejection cycle has to be employed. The result of such a measurement (performed with a buffer gas pressure of $p_{\mathrm{He}} = 1{\cdot}10^{-2}$ mbar) is shown in the bottom part of Fig. 18. Plotted as a function of the platform voltage are the average number of $^{132}Xe^{+}$ ions per cycle extracted from the buncher and detected by the MCP detector. It should be noted that the optimum value for the platform potential has shifted by about 25 eV, which means that a maximum capture efficiency requires an injection of the ions at an energy slightly lower than that for best transmission.

### *6.1.2 Radiofrequency parameters*

Both, the amplitude and the frequency of the RF potential should have an effect on the ion transmission through the linear trap and on the storage of the ions. Due to technical reasons, the frequency of the RF circuit used in this work was fixed to $\nu_{\mathrm{RF}} \approx 1$ MHz. Therefore, only measurements on the effect of a change of the RF amplitude were performed. The result of such a measurement is shown in Fig. 19. The upper part shows an injection and transmission measurement similar to those described above. The ion current at the end of the structure is plotted as a function of the amplitude $U_{\mathrm{RF}}$ of the applied radiofrequency. As expected, the transmission steadily increases with increasing amplitude (and deeper radial pseudopotential). Above $U_{\mathrm{RF}} \approx 120$ V, the transmitted current saturates. The lower figure shows the result of a measurement where the Xe ions are accumulated, cooled ($p_{\mathrm{He}} = 1 \cdot 10^{-2}$ mbar) and ejected. Shown is the number of detected ions as a function of $U_{\mathrm{RF}}$. It can be seen that a certain threshold amplitude of $U_{\mathrm{RF}} \approx 75$ V is required in order to obtain ions from the trap. The reason is that for too low RF amplitudes, the defocusing radial part of the DC potential at the axial potential minimum of the trap is stronger than the generated pseudopotential, as explained in section 3.1. The ions are transmitted to the "trapping" region where they are finally lost radially. Using (6) and the actual trap parameters, one obtains a threshold amplitude of $U_{\mathrm{RF,min}} \approx 60$ V which is in good agreement with the experimentally observed value.

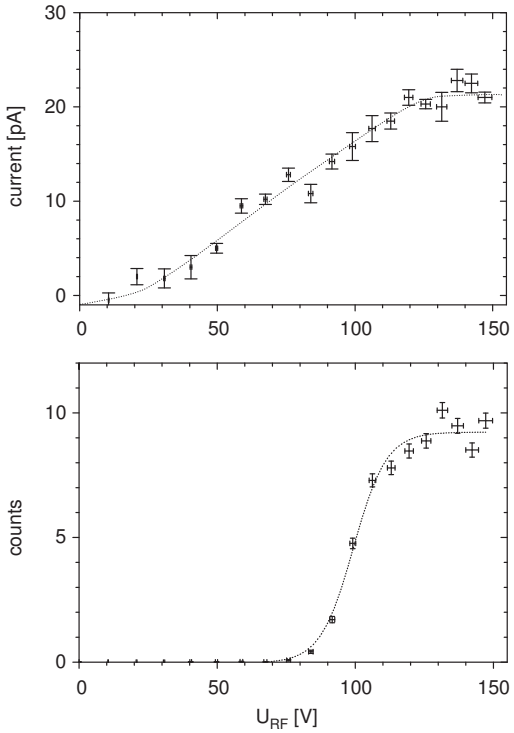


Fig. 19. Transmission of $^{132}Xe^{+}$ through the cooler and buncher (top) and number of accumulated and ejected ions (bottom) as a function of the radiofrequency amplitude $U_{\mathrm{RF}}$. The lines shown serve to guide the eye.

### *6.1.3 Buffer gas pressure*

The accumulation of the ions in the linear ion trap requires sufficient energy dissipation in the buffer gas (see Fig. 3) and hence a high enough pressure. If the pressure is too low, then most of the ions will hit the exit electrode of the linear ion trap and are lost. Figure 20 shows the number of ions ejected from the trap for constant injection conditions as a function of the gas pressure. It can be seen that a He pressure of a few $10^{-3}$ mbar is required in order to observe any ions. Above $p_{\mathrm{He}} \approx 10^{-2}$ mbar the number that can be extracted starts to saturate.

## *6.2 Efficiency*

After finding good parameters for the operation of the cooler and buncher the efficiency of the system was determined. From a current measurement as shown in Fig. 18 (top) and a comparison with the beam current measured with the Faraday-cup in front of the system, its injection and guiding efficiency $\epsilon_{\mathrm{trans}}$ was determined. Such measurements have been carried out with ISOLDE beams from various ion sources. Values for the transmission $\epsilon_{\mathrm{trans}}^{\mathrm{exp}}$ between 20% and 40% were found. This is in good agreement with the theoretical value of

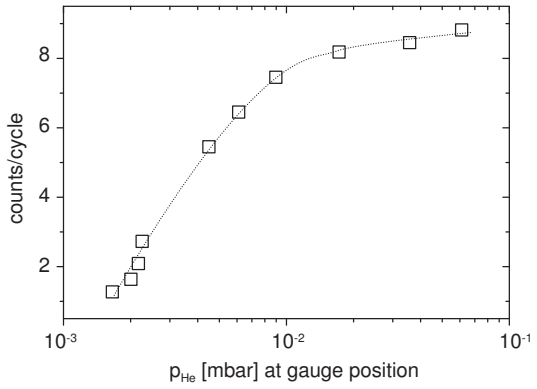


Fig. 20. Number of accumulated and ejected $^{208}Pb^{+}$ ions as a function of the buffer gas pressure $p_{\mathrm{He}}$. The value is the (He-corrected) reading of the gauge at the vacuum chamber containing the linear ion trap. The line shown serves to guide the eye.

$\epsilon_{\mathrm{trans}}^{\mathrm{theo}} \approx 35\,\%$ (see Section 3.3.1).

Most interesting is the total efficiency $\epsilon_{\mathrm{total}}$ of the cooler and buncher, which is defined as the ratio of the number of ions injected into the system and the number of ions finally counted in the extracted ion pulse. The measurements are performed in the following way: an attenuated ISOLDE beam, but still intense enough to perform a reliable current measurement (typically a few pA), is transported to the apparatus. For the injection into the buncher, a very short opening time for the ISOLDE beam gate is used in order to inject only a well defined small number of ions $N_{\mathrm{ion}}$ into the buncher. These ions are accumulated, cooled, ejected, and finally detected with the MCP detector. As mentioned above, this detector, which is normally only used for simple monitoring purposes, is not equipped with an electron-repelling grid. Therefore, according to [28], only about half of the maximum possible efficiency of $\approx 50$ % is achieved in the case of moderately heavy ions with 2.5 keV energy. With the number of counted events being $N_{\mathrm{MCP}}$ and an efficiency $\epsilon_{\mathrm{MCP}} \approx 30\,\%$, the overall efficiency is given by $\epsilon_{\mathrm{total}} = (N_{\mathrm{MCP}}/\epsilon_{\mathrm{MCP}})/N_{\mathrm{ion}}$.

Total efficiency measurements have been performed for various Xe isotopes and values of $\epsilon_{\mathrm{total}} \approx 12 \ldots 15\,\%$ were achieved. This value allows to study ions from the weakest radioactive beams available at ISOLDE with the ISOLTRAP spectrometer. However, compared to the efficiency $\epsilon_{\mathrm{trans}}$ for injection and transmission, the total efficiency $\epsilon_{\mathrm{total}}$ is lower by a factor of two to three. Storage time measurements for alkali ions have shown lifetimes of up to several 100 ms. For Xe ions as used for the efficiency measurement, no significant charge exchange with gas impurities has been observed, which could have caused ion loss. A possible explanation is that the MCP efficiency is lower than assumed. It is also likely that an optimal match of ISOLDE beam emittance and buncher acceptance has not yet been achieved. This will be investigated in forthcoming test measurements accompanied by further beam injection simulations.

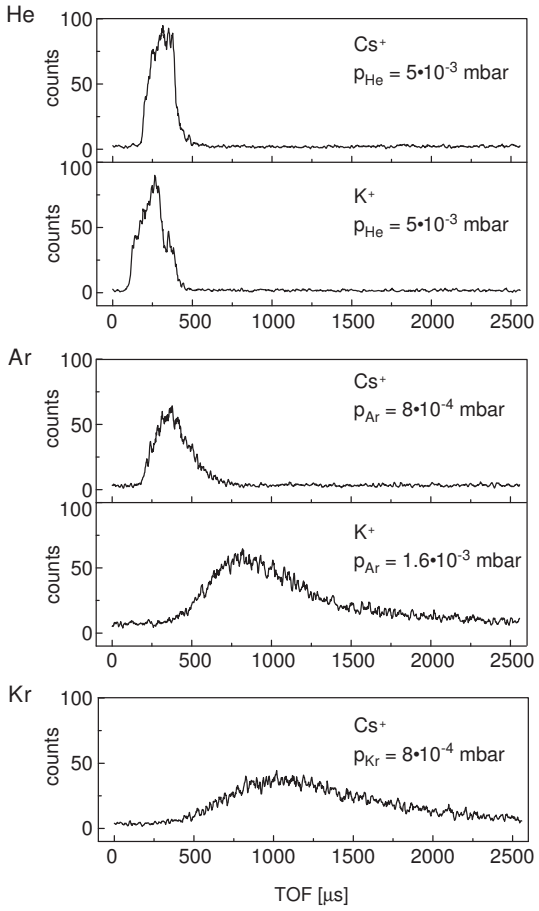


Fig. 21. Time structure of pulses of different ions after passage through the RFQ system for different buffer gases. Here, the ion trap was operated as an ion guide.

### *6.3 Cooling and beam emittance*

#### *6.3.1 Damping of ion motion and cooling*

In order to illustrate the damping of the axial ion motion in the cooler and buncher for different ions and types of buffer gas, very short ion pulses have been injected. The DC potential of the cooler was permanently set to the extraction mode, which means that the ions were directly accelerated to the MCP detector after a single passage through the system.

The result of such a measurement for various ion species and gases is shown in Fig. 21. With buffer gas of higher mass, the ion pulses arrive considerably later and are broadened. This can be understood by looking at the microscopic beam simulations shown in Fig. 4. There the trajectories show a significant scattering also for the axial motion. In the experiment the transmission of $^{39}K^{+}$ ions through $^{84}Kr$ was also tried, but, as expected no ion was able to reach the detector.

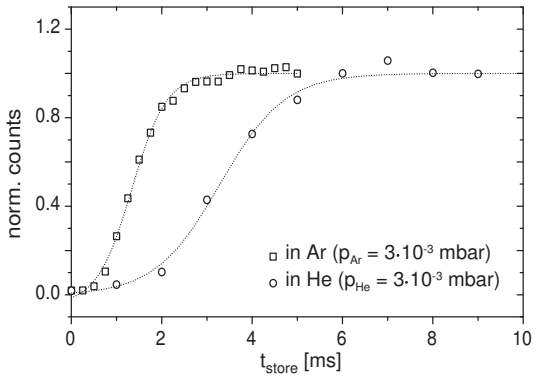


Fig. 22. Normalized number of $^{133}Cs^+$ ions extracted from the trap as a function of the storage time inside the trap. The measurements were performed with helium and argon as buffer gas.

An illustration of the transverse cooling process as a function of time is given in Fig. 22. In the experiment, $^{133}Cs^+$ ions were injected into the linear trap for a short period $T_{\mathrm{accu}} = 2\mu$s. The figure shows the number of ions ejected out of the trap as a function of the cooling time $T_{\mathrm{cool}}$ after injection. This measurement was performed for helium and argon as buffer gases at about the same pressure. For short cooling times, the number of ions that can be extracted is small and only above $T_{\mathrm{cool}} > 300\mu$s is the maximum number reached. This is because at the pressure of $p_{\mathrm{He}} \approx 3 \cdot 10^{-3}$ mbar used here several oscillations are required inside the trap before the radial extent of the ion cloud is smaller than the radius of the extraction hole. The figure also illustrates that stronger damping, and as a consequence faster cooling, is provided by the heavier buffer gas.

Figure 23 illustrates once more the axial cooling process. In the top figure the temporal width of the ejected ion pulse is shown as a function of the cooling time for the case of $^{39}K^+$ ions and $p_{\mathrm{He}} = 2.5 \cdot 10^{-3}$ mbar. As can be seen in the figure, an exponential decrease of the pulse width with time is observed. The pulse width decreases with decreasing ion temperature and smaller axial distribution of the ions in the trap. The width is therefore a good indicator of the ion temperature. The time constant $\tau_{\mathrm{cool}}$ of the curve can to first order be regarded as a measure of the cooling time constant. The value of $\tau_{\mathrm{cool}} = 0.5$ ms obtained in the measurement shown in Fig. 23 is comparable to a value of 0.3 ms calculated from ion mobility data and an estimate of the pressure inside the buncher close to the trapping region of $p \approx 10^{-2}$ mbar. Figure 23 also shows that the cooling time of the ions in the trap should be several times $\tau_{\mathrm{cool}}$ in order to extract ion pulses with minimum temperature out of the trap. The bottom part of Fig. 23 shows the measured time constants $\tau_{\mathrm{cool}}$ for Cs and K ions as a function of the pressure. For the highest pressures, time constants down to a few hundred microseconds are observed.

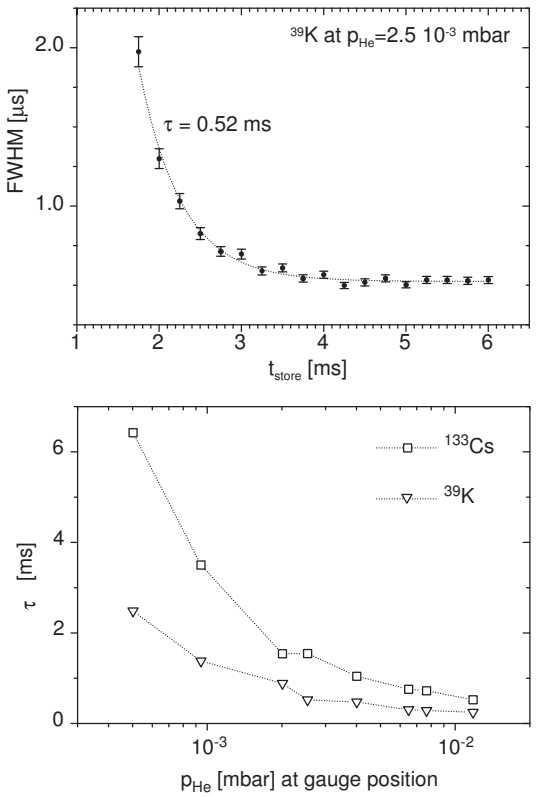


Fig. 23. Top: temporal width of ejected $^{39}$K ion pulses as a function of the storage time inside the trap. An exponential is fitted to the data. Bottom: time constants obtained as shown in the top figure as a function of the helium buffer gas pressure for K and Cs ions.

### *6.3.2 Cooling limit and emittance*

For a determination of the final ion temperature both in the axial and radial direction, two kind of measurements have been carried out. In both cases, ions were accumulated and cooled for $T_{\mathrm{cool}} = 20\,\mathrm{ms}$ to reach their equilibrium temperature.

For the determination of the axial temperature, the number of ions in a pulse has been measured temporally resolved with the MCP detector. The measured shape of the ion pulse can be compared to calculated shapes based on ion distributions at different temperatures. Such pulse shapes are shown in the top part of Fig. 24 for $^{133}$Cs ions extracted from the linear trap and accelerated to 30 keV. The data are plotted with respect to the time of ejection from the trap. The points correspond to the experimental data, the curves to calculated shapes for ion distributions with temperatures of 300 K, 500 K, and 800 K. A good agreement is achieved for a temperature of 300 K giving evidence that the ions reach the temperature of the buffer gas. This is in accordance with the predictions of Fig. 5. The bottom part of Fig. 24 shows the calculated energy distribution of the ejected ions. For the calculation, the confirmed 300-K ion

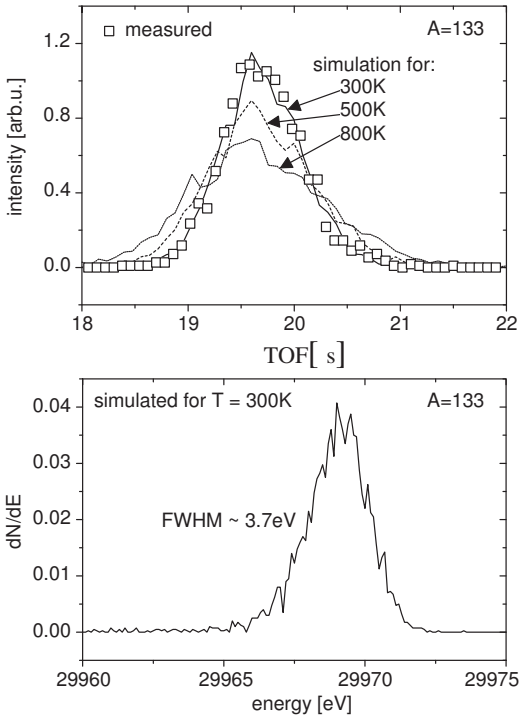


Fig. 24. Top: temporally resolved 30-keV ion pulse (squares) of $^{133}Cs^{+}$ ions compared to theoretical ion pulse shapes corresponding to initial ion temperatures of 300 K, 500 K and 800 K. The theoretical curves are normalized to the same number of ions. Bottom: calculated energy spectrum of the ion pulse corresponding to the 300-K pulse shape shown in the top figure.

distribution was taken together with the electric fields for the extraction as used in the experiment. From the time and energy spread of the ion pulses shown in the figure, a value for the longitudinal emittance of the ion pulse ejected from the buncher can be obtained. The total value is $\epsilon_{\mathrm{long}} \approx 10\,\mathrm{eV}\cdot\mu\mathrm{s}$.

The transverse temperature of the ions can be extracted from a beam emittance measurement. Such a measurement has been performed in the following way. The beam observation system was mounted at the 90° deflector chamber (Fig. 1 with the deflector removed). Ion pulses with an energy of 2.5 keV were created by using the pulsed cavity. With an einzel lens in front of the deflector chamber, the beam was focused onto the detector and the beam profile was observed with a CCD camera. The profile was found to be Gaussian-shaped with 90 % of the beam within a radius of about 1.8 mm. A beam scraper mounted on a linear feed-through at a distance of 500 mm in front of the beam viewing system was used to determine the size of the beam at this position. There a beam radius of 2.5 mm (corresponding to $> 90\,\%$ beam intensity) was observed. From this a beam divergence of 5 mrad is derived. Combining both measurements gives a rough upper limit for the transverse beam emittance of $\epsilon_{\mathrm{trans}} \approx 10\pi\,\mathrm{mm\,mrad}$.

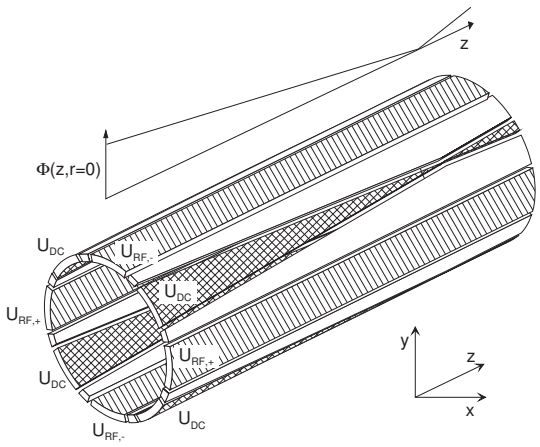


Fig. 25. Principle layout of a cylindrical radiofrequency quadrupole ion trap. Straight electrodes (line-hatched) are used to create the RF quadrupole field. An axial trapping potential is produced via tapered electrodes (cross-hatched) and corresponding ground electrodes (white). $\Phi(z, r = 0)$ sketches the expected potential on the axis of the cylinder.

If the extracted pulse was accelerated to 60 keV instead of 2.5 keV, it would have an emittance of about $2\pi$ mm mrad, which corresponds to more than tenfold improvement with respect to the original ISOLDE beam. This shows that gas-filled radiofrequency ion guides and traps can very effectively be used to improve the emittance of ion beams.

## 7 Future developments

A new type of radiofrequency quadrupole ion beam cooler and buncher has been investigated recently. It will be briefly discussed here while a comprehensive study including simulations will be presented in [25].

Figure 25 shows the principal layout of the system, which is based on a segmented cylinder. Four segments of constant width are used to create the radiofrequency quadrupole field by applying RF voltages $U_{\mathrm{RF}}$ with appropriate phases. An axial trapping potential $\Phi(z)$ is produced by applying DC-voltages $U_{\mathrm{DC}}$ to eight tapered electrodes, which are placed between grounded counter electrodes. For the ejection of accumulated ions, the voltage applied to the four short tapered electrodes is switched to a lower value.

The advantage of this system is, compared to the present system, that the RF and DC voltage supplies are decoupled and no matching circuit like the one shown in Fig. 16 is needed. Furthermore, only four electrical feedthroughs are required for the system shown in Fig. 25. However, higher RF and DC voltages have to be applied, which will require a very careful design of the electrodes.

Information gained from the present setup, from additional ion optical simulations, and from voltage breakdown tests with prototype electrode systems will be used as input for a detailed design of such a new simplified system of the ISOLTRAP ion beam cooler and buncher.

## 8 Conclusions and Outlook

In the work presented here, we have demonstrated for the first time the accumulation, bunching, cooling and emittance improvement of radioactive ion beams from an on-line mass separator by means of a linear radiofrequency ion trap. The efficiency of the system and the properties of the energy-variable ion bunches are in agreement with the theoretical expectations.

Compared to the previously used Paul trap system [18], the efficiency of ISOLTRAP has been increased by three orders of magnitude. This enables ISOLTRAP to be applied to very exotic isotopes with low production rates. First measurements of this kind have already been successfully performed. The investigation of the masses of neutron-deficient mercury isotopes was extended to $A = 182$ [25]. A mass measurement of the very short-lived ($T_{1/2} = 173\,\mathrm{ms}$) isotope $^{33}$Ar became possible [29], delivered by ISOLDE with an intensity of only a few thousand atoms per second. With this increased sensitivity, a very fruitful mass measurement program will be possible in the future.

The work has again confirmed that the concept of using trapping techniques to manipulate radioactive ion beams is very successful. Based on the experience with the present linear ion trap system we study now the design of a larger beam buncher for the preparation of short low-emittance ion pulses with close to 100 % efficiency. With a pulsed cavity as used in this work, the energy of the pulses can easily be varied from nearly zero up to more than 100 keV. The variability of this energy is expected to be very useful for nuclear-decay study experiments, laser spectroscopy experiments on unstable isotopes, as well as for solid-state and surface physics studies using radioactive probes.

Furthermore, the use of linear radiofrequency quadrupole ion accumulators, coolers and bunchers will play an important role in schemes presently discussed for the stopping of relativistic beams of nuclear reaction products and their conversion into low-energy ion beams.

## Acknowledgements

The authors wish to thank J. Bernard, W. Hornung, G. Marx and W. Quint at GSI Darmstadt, F. Ames and P. Schmidt from the university of Mainz and the CERN summer students S. Lindner, S. Harto, and C. Richter for their valuable help during the development and commissioning of the system. This work was partly carried out within the EXOTRAPS project in the EU LSF-RTD program and financially supported under contract number ERBFMGECT980099. It was also supported by NSERC of Canada.

## References

[1] G. Bollen, Nucl. Phys. **A616** (1997), 457c–468c.

[2] R. B. Moore und G. Rouleau, J. Mod. Optics **39** (1992), 361.

[3] H. Raimbault-Hartmann et al., Nucl. Instr. and Meth. **B126** (1997), 378.

[4] E. Teloy and D. Gerlich, Chem. Phys. **4** (1974), 417–427.

[5] D. Gerlich, Adv. Chem. Phys. **82** (1992), 1–176.

[6] Y. Kudryavtsev et al., Rev. Sci. Instrum. **69** (1998), 738–740.

[7] S. Fujitaka et al., Nucl. Instr. and Meth. **B126** (1997), 386–391.

[8] H. Penttilä et al., Nucl. Instr. and Meth. **B126** (1997), 213–217.

[9] G. Savard, Argonne National Laboratory, private communication.

[10] H. Backe et al., Nucl. Instr. and Meth. **B126** (1997), 406–410.

[11] E. Kugler et al., Nucl. Instr. and Meth. **B70** (1992), 41–49.

[12] G. Bollen et al., Nucl. Instr. and Meth. **A368** (1996), 675–697.

[13] G. Savard et al., Phys. Lett. **A158** (1991), 247.

[14] M. König et al., Int. J. Mass Spectr. Ion. Proc. **142** (1995), 95.

[15] St. Becker et al., Int. J. Mass Spectr. Ion. Proc. **99** (1990), 53.

[16] D. Beck et al., Nucl. Phys. **A626** (1997), 343c.

[17] F. Ames et al., Nucl. Phys. **A651** (1999), 3.

[18] S. Schwarz, Ph.D. thesis, Johannes Gutenberg University, Mainz, 1999, ISBN 3-8288-0735-6.

[19] M.D. Lunney and R.B. Moore, Int. J. Mass Spectrom. Ion Proc. **190/191** (1999), 153–160.

[20] A. Kellerbauer et al., submitted to Nucl. Instr. Meth. A.

[21] P.H. Dawson, *Quadrupole Mass Spectrometry*, Elsevier, Amsterdam, 1976.

[22] W. Paul, Review of Modern Physics **62** (1990), 531–540.

[23] H.G. Dehmelt, Adv. At. Mol. Phys. **3** (1967), 53–72.

[24] E.W. McDaniel and E.W. Mason, *The Mobility and Diffusion of Ions in Gases*, Wiley, 1973.

[25] S. Schwarz et al., to be published.

[26] H. Wollnik, J. Brezina, and M. Berz, Nucl. Instr. and Meth. **A258** (1987), 408–411.

[27] J.M. Meek and J.D. Craggs, *Electrical Breakdown of gases 1st ed.*, Oxford publishing, 1953.

[28] B. Brehm et al., Meas. Sci. Technol. **6** (1995), 953–958.

[29] F. Herfurth et al., to be submitted to Phys. Rev. Lett.